Journal of Proteomics 310 (2025) 105336

Contents lists available at ScienceDirect

Journal of Proteomics

journal homepage: www.elsevier.com/locate/jprot

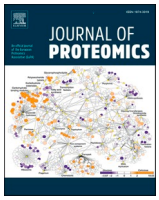

# Untargeted metabolomics of 3xTg-AD neurotoxic astrocytes

Diego Carvalho [a,b], Pablo Diaz-Amarilla [c,1], Mathew R. Smith [d,e], María Daniela Santi [c,f], Marcela Martinez-Busi [g], Young-Mi Go [d], Dean P. Jones [d], Pablo Duarte [c], Eduardo Savio [c], Juan A. Abin-Carriquiry [a,h,**], Florencia Arredondo [a,c,*]

[a] Departamento de Neuroquímica, Instituto de Investigaciones Biológicas Clemente Estable (IIBCE), Montevideo, Uruguay
[b] Área de Matemática - DETEMA, Facultad de Química, Universidad de la República, Montevideo, Uruguay
[c] I&D Biomédico y Químico Farmacéutico, Centro Uruguayo de Imagenología Molecular (CUDIM), Montevideo, Uruguay
[d] Division of Pulmonary, Allergy, Critical Care and Sleep Medicine; Department of Medicine, Emory University, GA, USA
[e] Atlanta Veterans Affairs Healthcare System, Decatur, GA, USA
[f] Instituto Multidisciplinario de Biología Vegetal (IMBIV-CONICET), Ciudad Universitaria. X5000HUA, Córdoba, Argentina
[g] Plataforma de Servicios Analíticos, Instituto de Investigaciones Biológicas Clemente Estable, Montevideo, Uruguay
[h] Laboratorio de Biofármacos, Instituto Pasteur de Montevideo, Montevideo, Uruguay

ARTICLE INFO

*Keywords:*
Metabolomics
Alzheimer's disease
Dementia
3xTg-AD mouse
Astrocytes

ABSTRACT

Alzheimer's disease (AD) is the most common form of dementia, affecting approximately 47 M people worldwide. Histological features and genetic risk factors, among other evidence, supported the amyloid hypothesis of the disease. This neuronocentric paradigm is currently undergoing a shift, considering evidence of the role of other cell types, such as microglia and astrocytes, in disease progression. Previously, we described a particular astrocyte subtype obtained from the 3xTg-AD murine model that displays neurotoxic properties in vitro. We continue here our exploratory analysis through the lens of metabolomics to identify potentially altered metabolites and biological pathways.

Cell extracts from neurotoxic and control astrocytes were compared using high-resolution mass spectrometry-based metabolomics. Around 12 % of metabolic features demonstrated significant differences between neurotoxic and control astrocytes, including alterations in the key metabolite glutamate. Consistent with our previous transcriptomic study, the present results illustrate many homeostatic and regulatory functions of metabolites, suggesting that neurotoxic 3xTg-AD astrocytes exhibit alterations in the Krebs cycle as well as the prostaglandin pathway.

This is the first metabolomic study performed in 3xTg-AD neurotoxic astrocytes. These results provide insight into metabolic alterations potentially associated with neurotoxicity and pathology progression in the 3xTg-AD mouse model and strengthen the therapeutic potential of astrocytes in AD.

*Biological significance:* Our study is the first high-resolution metabolomic characterization of the novel neurotoxic 3xTg-AD astrocytes. We propose key metabolites and pathway alterations, as well as possible associations with gene expression alterations in the model. Our results are in line with recent hypotheses beyond the amyloid cascade, considering the involvement of several stress response cascades during the development of Alzheimer's disease. This work could inspire other researchers to initiate similar studies in related models. Furthermore, this work illustrates a powerful workflow for metabolite annotation and selection that can be implemented in other studies.

## 1. Introduction

Alzheimer's disease (AD) is a neurodegenerative pathology characterized by memory loss, spatial and temporal disorientation, and progressive cognitive impairment [1,2]. Histologically, it is characterized by the presence of amyloid plaques and neurofibrillary tangles as a

* Correspondence to: Florencia Arredondo, I&D Biomedico y Químico Farmacéutico, Centro Uruguayo de Imagenología Molecular (CUDIM), Montevideo, Uruguay.
** Correspondence to: Juan A. Abin-Carriquiry, Laboratorio de Biofármacos, Institut Pasteur de Montevideo, 11600 Montevideo, Uruguay.
*E-mail addresses:* aabin@pasteur.edu.uy (J.A. Abin-Carriquiry), florencia.arredondo@cudim.org (F. Arredondo).
[1] Deceased.

https://doi.org/10.1016/j.jprot.2024.105336
Received 10 July 2024; Received in revised form 17 October 2024; Accepted 19 October 2024
Available online 23 October 2024

result of extracellular deposition of amyloid beta protein and intraneuronal aggregation of hyperphosphorylated tau protein, respectively [1,2]. Although most cases are idiopathic, several genetic risk factors have been discovered, mainly related to the synthesis and processing of the amyloid protein [1,2]. This evidence is in line with the amyloid hypothesis, traditionally evaluated from a neuronocentric point of view. In this sense, an imbalance between the production and elimination of beta amyloid would trigger inflammatory and oxidative stress processes that would ultimately lead to the loss of synaptic integrity, neuronal connectivity and, ultimately, to progressive regional neurodegeneration [3].

Although one of the main focuses of research has been the role of tau and beta amyloid protein aggregates in neuronal death, it is well known that the pathology of AD is multifactorial and involves an interaction of many risk factors and processes such as vascular pathology, inflammation and metabolic alterations [4–6]. This has led to the need to further study the role of other important cellular players such as glia and their associated processes. In particular, astrocytes are glial cells that have key functions in brain homeostasis, such as synapse regulation, trophic supply, and waste removal, among others [7]. Astrocytes respond to tissue damage by assuming different phenotypes widely known as astrocyte reactivity or astrogliosis [8]. In this sense, multiple studies point to early imbalances in astrocyte function and morphological changes associated with the progression of AD, as well as their contribution to both neuroinflammation and neuroprotection in various diseases and brain models [9–13].

Transgenic mouse models are invaluable tools to improve our understanding of diseases. In the present work we use the 3xTg-AD mouse model of AD, which replicates many features of the disease, including plaque and tangle pathology, age-related cognitive deficits, astrocyte reactivity, and brain atrophy. In previous studies, we isolated and cultured astrocytes from the cortex and hippocampus of 10-month-old symptomatic 3xTg-AD mice that exhibited a high proliferation rate, differential expression of astrocyte markers, and the ability to mediate neuronal degeneration [14]. The results added evidence to the hypothesis that microenvironment-induced changes in astrocyte function during disease progression may promote or accelerate neurodegeneration.

In the present work we expand the description of these neurotoxic astrocytes through the metabolomic lens. Metabolomics is an emerging discipline interested in the study of the global collection of small molecules in the body or cells that reflects the combined effect of genetic factors and environmental exposures on phenotype [15]. In particular, untargeted approaches do so without a priori knowledge of the metabolites involved. A currently untargeted high-resolution metabolomics strategy typically involves the use of liquid chromatography coupled with high-resolution mass spectrometry to accurately separate and detect the mass and abundance of distinct metabolic features. We used this approach to identify metabolites and altered metabolic pathways in neurotoxic 3xTg-AD astrocytes. We then validated changes in key metabolic centers using a targeted approach. In addition to meeting growth and energy demands, metabolites regulate systemic functions such as inflammation [16,17]. The current results illustrate these characteristics. Pathway analysis suggested a number of associated biological processes, mainly related to amino acid and central carbon metabolism, as well as arachidonic acid metabolism. Furthermore, metabolome-transcriptome associations supported these findings [18].

## 2. Methods

### 2.1. Animals

The animal procedures were approved by the Institutional Animal Ethics Committee (CEUA-CUDIM) in accordance with the international guidelines followed by the National Animal Experimentation Committee (CNEA) for the use of live animals. As in previous work, both female homozygous 3xTg-AD (B6;129-Tg(APPSwe, tauP301L)1Lfa Psen1$^{(tm1Mpm)}$/Mmjax strain) [19] and female non-transgenic wild-type (non-Tg) mice (C57BL/ 6 J) (The Jackson Laboratory) were raised and housed in a CUDIM SPF centralized animal facility with a 12-h light-dark cycle and ad libitum access to food and water [14].

### 2.2. Astrocyte cultures from adult and neonatal mice

Neurotoxic astrocyte cultures were prepared from the cerebral cortex and hippocampus of 9- to 10-month-old 3xTg-AD female mice according to previously described methods [14]. Female animals were used since sex differences in the development of the pathology have been described in this AD murine model, with a greater expression of transgenes in females [20,21]. Astrocytes isolated from 9- to 10-month-old non-Tg mice were not used as controls in our studies due to the low yield achieved [14]. Instead, astrocytic cultures derived from neonatal non-Tg mice as well as astrocytes from neonatal 3xTg-AD mice were used as controls. These non-toxic controls allowed us to assess whether astrocytes from this mice model of AD exhibit alterations when isolated before the disease onset. Nontoxic control astrocyte cultures were derived from the cerebral cortex and hippocampus of neonatal (postnatal day 0–2) 3xTg-AD and non-Tg (C57BL/6 J) mice following the methods described by Cassina et al. with minor modifications [14,22]. All cell cultures were amplified and maintained at 37 °C in a humidified incubator with 5 % $CO_2$.

### 2.3. Sample collection and preprocessing

Extraction of metabolites from cultured cells was performed based on previous work by Go et al. (2015), Liu et al. (2019), as well as Sapcariu et al. (2014) [23–25]. One sample consisted of metabolites extracted and pooled from 3 wells of a 6-well plate, pooling a total of 9 samples per condition. Briefly, confluent cells were washed with 0.9 % (m/v) NaCl at room temperature, followed by the addition of 300 μL of an ice-cold HPLC-grade acetonitrile-water solution mixture (1:2) per well. This allowed us to scrape cells, precipitate proteins, and extract metabolites. The extracts were kept at 4 °C for 30 min. and centrifuged at 16,100*g* for 10 min to remove the protein and any remaining insoluble fraction. Supernatants were transferred to screw-cap vials and dried in a fast vacuum centrifuge (overnight, 35 °C).

### 2.4. High-resolution mass spectrometry-based metabolomics

Dried samples were reconstituted with 300 μL of 1:2 HPLC grade water: acetonitrile solution mixture containing internal isotopic standard mixture [26,27]. Samples were mixed (10 s vortex) and shaken at 4 °C (overnight) before centrifugation to remove any remaining protein. The resulting supernatant was transferred to low-volume autosampler vials, kept at 4 °C, and analyzed in triplicate. Supernatants were analyzed using a High-Field Q-Exactive Orbitrap instrument (ThermoFisher; Waltham MA) coupled to a Thermo Dionex Ultimate 3000 liquid chromatography system (120,000 resolution with scan range 85–1275 *m/z*). We utilized a dual-column chromatography pipeline, the first being a HILIC column (hydrophilic interaction liquid chromatography; ThermoFisher Scientific, Accucore, 50 × 2.1 mm, 2.6 μm) operated in parallel to our second column, a reverse phase column (C18; Higgins Analytical, 50 × 2.1 mm, 2.6 μm) for simultaneous analytical separation on one column while flushing of the other. Dual electrospray ionization (ESI) was used for analysis with positive ESI for the HILIC column (HILIC+), and negative ESI was used with the C18 reverse phase column (C18-). A sample volume of 10 μL was injected for analysis on each column. The flow rate of the HILIC column was maintained at 0.35 mL/min until 1.5 min, increased to 0.4 mL/min at 4 min and held for 1 min, resulting in a total analytical run time of 5 min. Mobile Phases A and B were LCMS grade water and acetonitrile, respectively. Mobile phase C was composed of 2 % formic acid (*v*/v) in water. Mobile phase

conditions consisted of 22.5 % A, 75 % B, 2.5 % C which was held for 1.5 min, with a linear gradient to 77.5 % A, 20 % B, 2.5 % C at 4 min, and held for 1 min. The HILIC column was then flushed for 5 min with a wash solution of 77.5 % A, 20 % B, 2.5 % C. For the reverse-phase C18 column, the flow rate was maintained at 0.4 mL/min for 1.5 min and was then increased to 0.5 mL/min at 2 min and held constant for 3 min. Mobile Phases A and B were LCMS-grade water and acetonitrile, respectively. Mobile phase C was 10 mM ammonium acetate in water. Mobile phase conditions for the C18 column were 60 % A, 35 % B, 5 % C for 0.5 min, with a linear gradient to 0 % A, 95 % B, 5 % C starting at 1.5 min, and held for 3.5 min, resulting in a 5 min run. The reverse phase column was flushed with 0 % A, 95 % B, 5 % C for 2.5 min, followed by an equilibration solution of 60 % A, 35 % B, 5 % C for the remaining 2.5 min. Collected mass spectral data were analyzed for features using Xcaliber (ThermoFisher; Waltham MA). Ultra-high resolution mass spectrometry operating at 60,000 and 120,000 resolution has previously been shown to provide effective metabolite quantification in biological extracts [28] and the use of complementary chromatography and ionization phases have been shown to improve the detection of endogenous and exogenous chemicals. Raw data is available at the NIH Common Fund's National Metabolomics Data Repository (NMDR) website, the Metabolomics Workbench, https://www.metabolomicsworkbench.org where it has been assigned Study ID ST003515. The data can be accessed directly via its Project DOI: https://doi.org/10.21228/M8DR6G [29].

### 2.5. Metabolomics data processing and statistical analysis

Raw mass spectral data files were converted to computable document format (CDF) using Xcalibur file conversion software (Thermo Fisher Scientific, San Diego, CA) for further processing. Data were processed for peak extraction, noise filtering, *m/z* and retention time alignment, and quantification of ion intensities using apLCMS [30] with enhanced data extraction using xMSanalyzer [31]. xMSanalyzer improves feature detection through systematic data re-extraction, statistical filtering and fusion [31]. Metabolite feature values were summarized by the median in triplicate and subjected to quality assessment. The samples were filtered considering an overall Pearson correlation of technical replicates of (r) $> 0.70$ and a cut-off coefficient of variation of 75 %. Considering the number of missing values, one sample outlier was further removed from the C18 and HILIC cell extraction feature tables. Data were log2 transformed and quantile normalized for subsequent analyses. Log transformation reduces heteroscedasticity, so that each metabolite has a mean of 0 and a standard deviation of 1, and quantile normalization reduces variability between samples [32]. Then, the obtained data sets were used for statistical analysis.

Principal component analysis (PCA) was performed using R packages implemented on the MetaboAnalyst server to visualize the cluster distribution according to the variation in feature intensity patterns between samples. Selection of differentially expressed *m/z* features was performed using linear model for microarray data analysis (LIMMA) [33]. A Benjamini-Hochberg false discovery rate (FDR) of 20 % was then applied to adjust for multiple comparisons and identify those metabolites of greatest interest [34]. To visualize the distributions of differentially expressed features, a colour-coded heat map with two-way hierarchical cluster analysis (HCA) was performed using the hclust function in R to determine the clustering pattern of selected samples and *m/z* features.

All statistical and computational analysis was performed in R software (R Project for Statistical Computing, Vienna, Austria).

### 2.6. Metabolite feature annotation and pathway enrichment analysis

Metabolite features were annotated using two approaches. On the one hand, features were annotated by searching the metabolic databases of the Kyoto Encyclopedia of Genes and Genomes (KEGG) and the Human Metabolome Database (HMDB) for putative matches to known metabolites using the package R xMSannotator with *m/z* threshold (±5 ppm) [35–37]. xMSannotator uses a multilevel clustering procedure based on feature intensity across all samples, retention time, mass defect, isotope/adduct patterns, intensity correlations between samples, and knowledge of the biochemical pathways to assign confidence levels in the annotations [37]. We prioritize levels 2 (medium confidence) and 3 (high confidence). On the other hand, discriminant features were processed through Mummichog 2.0 (available in the public domain at http://mummichog.org/), a program that performs putative metabolite annotation and pathway enrichment analysis in a single step [38]. A biological process is expected to favor a more connected network rather than random distributions. This procedure then assigns putative metabolite matches based on which pathways are enriched within the metabolite set. Mummichog uses a reference model derived from the integration of the KEGG, UCSD Recon1 and Edinburgh human metabolic networks. Features that differed at $p < 0.05$ were selected, permutation tests ($p < 0.05$) were used in the pathway enrichment analysis, and a threshold of 5 ppm was used for feature matching. Significant pathways were selected if they included a minimum of 4 matching metabolites. The annotations were verified manually to verify consistency between both procedures. Some annotations were further supported based on comparison of adducts, *m/z* and retention time with an internal database of previously confirmed metabolites [25].

### 2.7. Evaluation of metabolome-transcriptome association with xMWAS

The presented metabolomic data were integrated with previous transcriptomic data ($n = 3$) of 3xTg-AD astrocytes using xMWAS, an integration program based on the sparse partial least squares (sPLS) regression method [39]. sPLS is a regression-based modeling approach that simultaneously performs variable selection and data integration [40]. Additionally, the software performs community detection (groups of nodes strongly connected to other nodes in the same community, but with sparse connections to the rest of the network) using the multilevel community detection algorithm [41]. All data were log-transformed, specifically transcriptomic data were also voom-normalized and metabolic features were quantile normalized. To compensate for the fact that these data sets came from different sample data tables, they were expanded to generate all possible combinations. The thresholds for determining significant associations were set as follows: correlation threshold $|r| > 0.6$ and $p < 0.05$ as determined by Student's *t*-test.

### 2.8. Targeted metabolite detection

Selected metabolites were validated by targeted detection [25]. Briefly, extracts from astrocytic cell cultures were processed as described above and the selected amino acids GABA and glutamate were detected using a UHPLC/MS Thermo scientific Ultimate 3000 RS coupled to a Thermo scientific ISQ™ EC single quadrupole mass spectrometer system, as done in previous work [42]. Samples were reconstituted in hydrochloric acid 0.1 M, and the mixture was centrifuged at 13,000 $\times g$ for 10 min at 4 °C. The supernatants were then filtered through cellulose acetate syringe filters (2.5 mm diameter, 0.22 μm pore size; GVS) and analyzed by UHPLC/MS, according to the method of Soo Hyun Park et al. (Thermo Scientific, application note 73,151) for separation and detection of amino acids in wine, with minor modifications. Modifications included the reduction of the flow of the mobile phase to 0.3 mL/min and the use of an injection volume of 5 μL. The mobile phase used was a mixture of mobile phase A, which contained 10 % of a 200 mM ammonium formate solution in acetonitrile at pH = 2.8 and a mobile phase B, which contained 10 % of a 200 mM ammonium formate solution in water at pH = 2.8. The mobile phase was injected during the run according to the gradient presented by Lozano et al. (2022) [42] (see Supplementary Table 3), while the detection was made using the single ion monitoring mode in the positive mode selecting an ion of *m/z* 104 corresponding to the value of m/z of GABA in its anionic form, and single ion monitoring mode in the negative mode selecting an ion of m/z

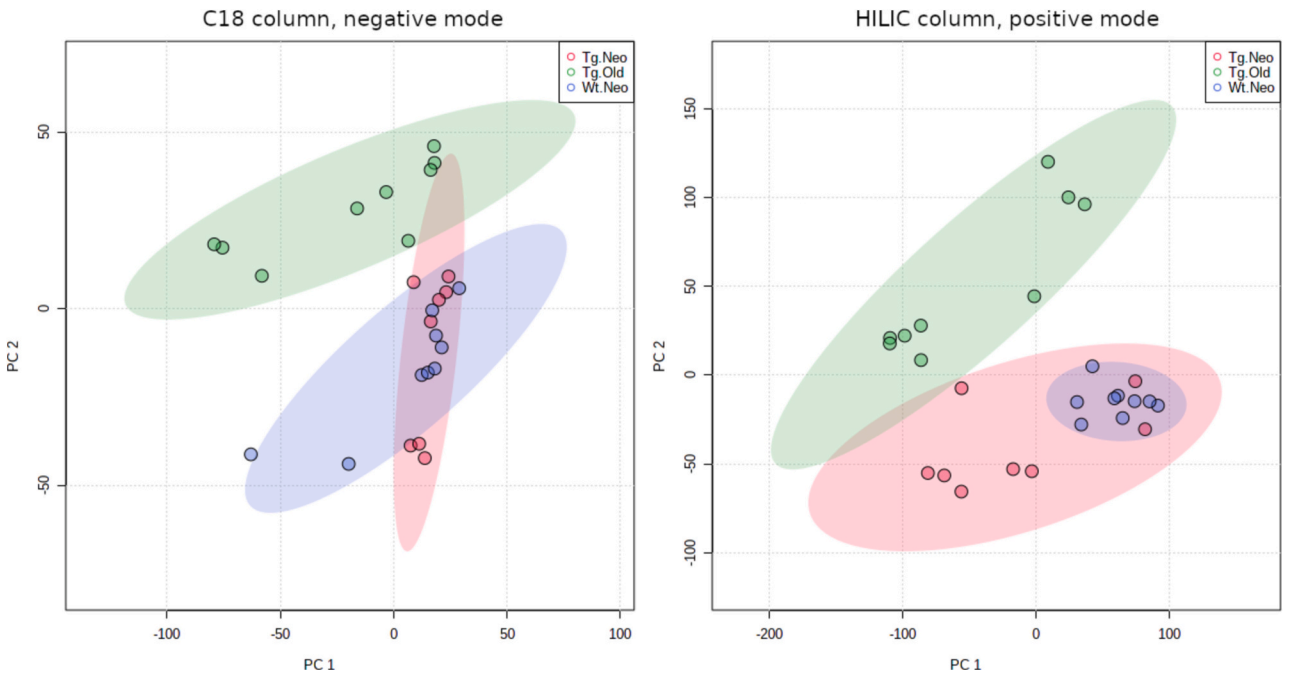


**Fig. 1.** Principal component analysis (score plot) of the metabolites detected in extracts of neurotoxic cells and neonatal astrocytes from the 3xTg-AD model. Left: metabolites detected with C18 column chromatography and negative ionization mode, right: metabolites detected with HILIC column chromatography and positive ionization mode. Figure rendered with the MetaboAnalyst server [43].

146.1 corresponding to the value of m/z of glutamate in its anionic form, respectively. The peaks obtained were analyzed and integrated with the Chromeleon™ Chromatography Data System (CDS) data processing software (Thermo Fisher Scientific, EU) version 7.2. The concentration values of the samples were calculated as the values of the areas of each peak divided by the dilution factor of the injection and interpolated with a standard injected in said run.

## 3. Results and discussion

### *3.1. Untargeted metabolomics distinguishes symptomatic astrocytes derived from 3xTg-AD mice from those obtained from presymptomatic 3xTg-AD neonates*

Untargeted metabolomics of cell extracts from neurotoxic "old" 3xTg-AD (Tg.Old), neonatal 3xTg-AD (Tg.Neo), and wild-type neonatal (Wt.Neo) astrocytes was performed under two analytical schemes: based on C18 column chromatography with negative ionization mode (C18-) and HILIC column chromatography with positive ionization mode (HILIC+), respectively. Although the focus of the present study is to assess metabolic changes that have arisen from age and disease progression but not from transgenesis per se, our initial experimental design also included astrocytes isolated from neonatal wild-type mice (Wt.Neo). Principal component analysis of the metabolites found in cell extracts detected features with discriminatory value, although they covered around 10 % of the observed variation, which could translate into a relatively small number of discriminant metabolites (Fig. 1). The remaining components include a similar amount of variation (not shown). As we did in our previous transcriptomic study of these neurotoxic astrocytes, we included Wt.Neo astrocytes as an additional control. As detected in that study, it can be observed that Wt.Neo and Tg.Neo astrocytes behave similarly (Fig. 1), presenting an almost complete overlap of all principal components of the score plot (not shown). Discriminatory features were evaluated by comparing Tg.Old astrocytes with Tg.Neo astrocytes.

Approximately 5 k and 6 k features detected in C18- and HILIC+ acquisitions respectively met the filtering criteria. Differentially expressed features were selected using LIMMA statistics with a lenient threshold of FDR < 0.2, resulting in around 400 and 1000 features from the C18- and HILIC+ datasets respectively. Heat maps of the C18- and HILIC+ data sets showed significant clustering of 3xTg-AD neurotoxic astrocytes separated from 3xTg-AD neonatal astrocytes, illustrating the reproducibility of the patterns within each group and their discriminant value (Fig. 2, top panel). The distribution of discriminative features along the *m/z* dimension can be visualized using Manhattan plots (Fig. 2, lower panel), which indicate chemical properties similar to the rest of the metabolic features in the data sets. Similar behavior can be observed along the retention time dimension (not shown). Approximately 36 % of the selected C18- features and 38 % of the selected HILIC+ features are upregulated.

### *3.2. Associations between altered metabolic and signaling pathways*

Mummichog pathway analysis was performed to identify altered biochemical pathways and obtain metabolite annotations for differentially expressed features potentially involved in them. Fig. 3 presents a list of pathways detected by this procedure. Taking into account the overlapping pathways, the results of the C18 data set can be summarized as pathways related to central carbon metabolism and the metabolism of amino acids such as *Glycine, serine, alanine and threonine*, *Glutamate metabolism*, and *Glycolysis and gluconeogenesis*. Results from the HILIC data set include pathways related to *Arachidonic acid metabolism* in addition to pathways related to amino acid metabolism. The identified pathways are among the most relevant centers of astrocyte metabolism, as will be discussed later. The annotations of the associated metabolites were complemented with the results from xMSAnnotator. Up to 100 differentially expressed features from the C18 and HILIC datasets were annotated with medium and high confidence levels (see Supplementary Table 1). The annotations were further supported by comparison with an internal list of previously validated metabolites [25], as presented in Table 1. These most reliable annotated metabolites illustrate and support previously found pathways.

As supporting evidence for the present results, we set out to more comprehensively study the associations between the current untargeted

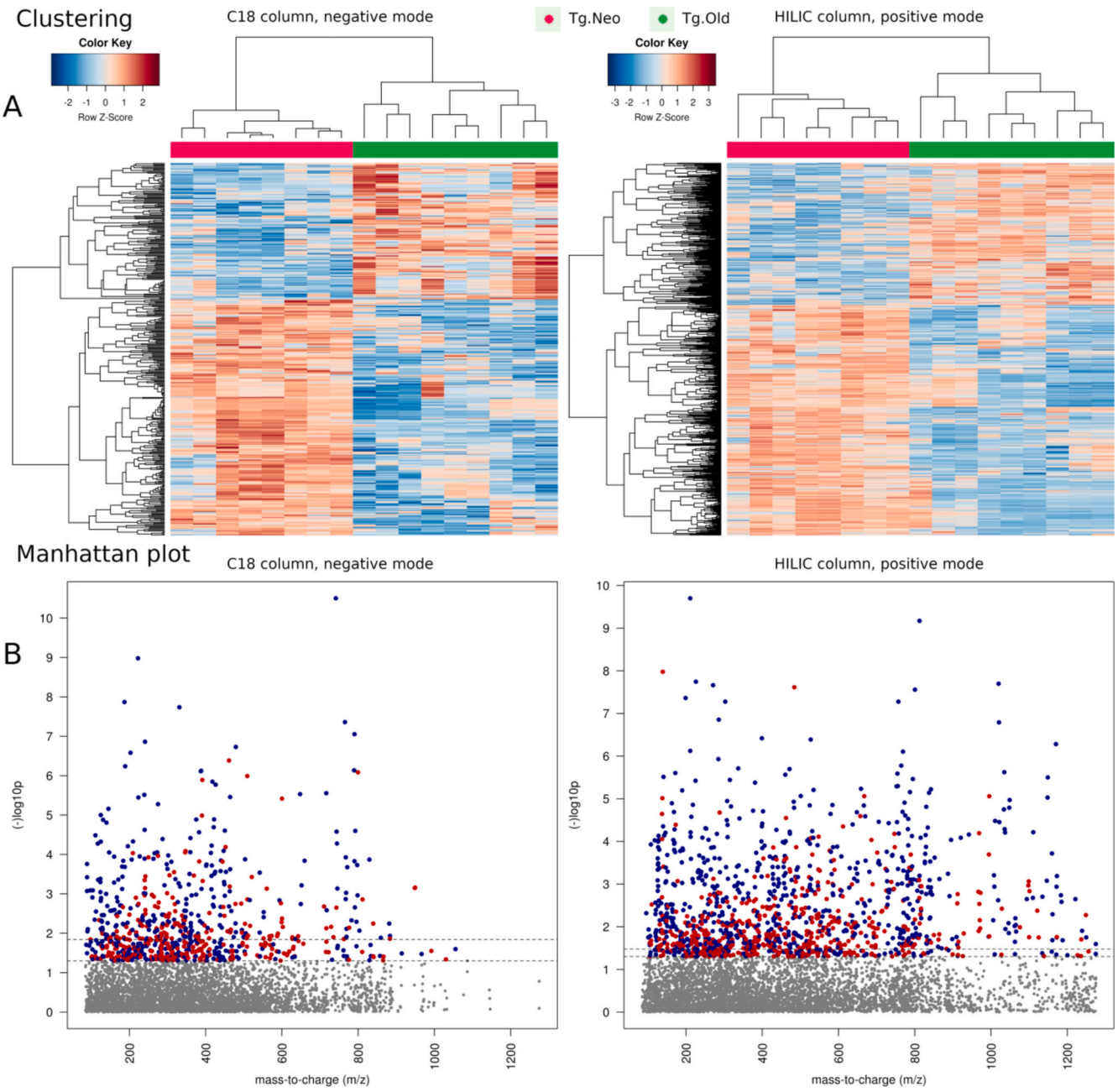


**Fig. 2.** Differentially expressed metabolic features detected in cell extracts from neurotoxic and neonatal astrocytes from the 3xTg-AD model (LIMMA analysis). A. Clustering analysis (all significant features in rows, samples in columns). B. Manhattan type 1 plot presenting the negative log10(*p*-value) of the metabolite features as a function of its mass/charge ratio. Left: metabolites detected with C18 column chromatography and negative ionization mode, right: metabolites detected with HILIC column chromatography and positive ionization mode. From bottom to top, features above the first dashed horizontal line were significant with a *p*-value $<0.05$, and above the second dashed line significant with a *q*-value (FDR) $<0.2$. A total of 382 features were selected from 5294 filtered features detected by C18 column chromatography and negative ionization mode. A total of 1041 features were selected from 6189 filtered features detected by HILIC column chromatography and positive ionization mode. Red: higher expression in neurotoxic astrocytes; blue: lowest expression. Abbreviation: LIMMA, linear models for microarray data. (For interpretation of the references to colour in this figure legend, the reader is referred to the web version of this article.)

metabolomics data and our previously reported gene expression data [18]. We specifically used the xMWAS multi-omics approach that can potentially identify concomitant or intertwined changes between different regulatory levels. Transcripts and correlated discriminant metabolites (differentially expressed genes, DEGs) were then obtained. The consistency of the xMWAS results with the previous analysis was verified by an overrepresentation analysis of DEGs on the STRING web server. Overrepresented KEGG pathways obtained from upregulated DEGs included *Protein processing in endoplasmic reticulum*, *RNA transport*, *Toll-like receptor signaling pathway*, *NF-kappa B signaling pathway*, *Toxoplasmosis*, *N-Glycan biosynthesis*, *Folate biosynthesis*; and of negatively regulated DEGs: *Adherens junction*, *Glycine, serine and threonine metabolism*, *Rap1 signaling pathway* and *cAMP signaling pathway*, among others. In this sense, the results are consistent with previous findings and highlight DEGs that could be involved in the metabolic pathways detected. Among these DEGs, the various metabolic enzymes included can be grouped into those related to the metabolism of fatty acids and related compounds (sphingolipids, glycosphingolipids, arachidonic acid), central carbon metabolism (oxidative phosphorylation, metabolism of amino acids, etc.), N-glycan and glycosaminoglycan

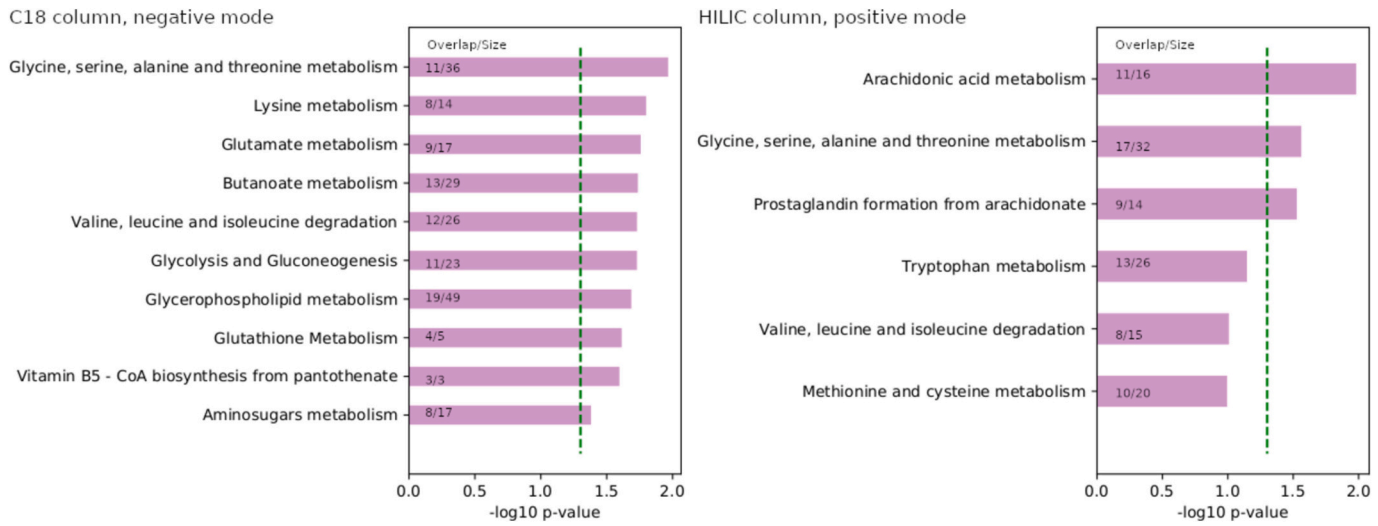


**Fig. 3.** Mummichog pathway analysis of differentially expressed metabolite features. Size corresponds to the total number of known metabolites in a given pathway, and overlap corresponds to the number of matching metabolic features that are differentially expressed. Pathways were considered to differ between groups if $p \leq 0.05$ and overlapped >4.

**Table 1**
Prevalidated cellular metabolites detected by high-resolution metabolomics. Annotations of selected metabolites are based on comparison with an internal database of previously confirmed metabolites (similar adduct, *m/z* and retention time) [25]. Pathway information compiled from Mummichog results and KEGG metabolite annotations.

| CELL METABOLITES | | | | | | | | |
|---|---|---|---|---|---|---|---|---|
| Chemical ID | Confidence | Mz | Time | *P* value | Max fold change (log2) | Name | Adduct | Pathways |
| C05984 | 2 | 103.0400 | 48.5 | 0.0012 | −0.93 | 2-Hydroxybutyrate | M-H | Butanoate metabolism |
| C03761 | 2 | 161.0456 | 50.9 | 0.0026 | −1.72 | 3-Hydroxy-3-methylglutarate | M-H | |
| C01879 | 3 | 130.0499 | 94.4 | 0.0004 | −1.82 | 5-Oxoproline | M + H | Glutathione metabolism |
| C06428 | 3 | 301.2175 | 191.7 | 0.0055 | 0.94 | Eicosapentaenoic acid | M-H | |
| C02693 | 2 | 175.0866 | 64.6 | 0.0292 | −0.80 | Indole-3-acetamide | M + H | Tryptophan metabolism |
| C00637 | 3 | 158.0611 | 78.3 | 0.0106 | −1.16 | Indoleacetaldehyde | M-H | Tryptophan metabolism |
| C00025 | 3 | 147.0490 | 33.7 | 0.0138 | 1.72 | L-Glutamate | M-H_[−1] | Glutamate metabolism |
| C00186 | 3 | 89.0244 | 46.1 | 0.0002 | −1.55 | L-Lactate | M-H | Glycolysis and gluconeogenesis |
| C00149 | 2 | 133.0143 | 46.4 | 0.0035 | −1.49 | L-Malate | M-H | Glycolysis and gluconeogenesis |
| C00065 | 2 | 106.0499 | 116 | 0.0165 | −2.27 | L-Serine | M + H | Glycine, serine and threonine metabolism |
| C00078 | 2 | 203.0826 | 50.2 | 0.0023 | −1.61 | L-Tryptophan | M-H | Glycine, serine and threonine metabolism |
| C00624 | 2 | 188.0565 | 35.9 | 0.0002 | −2.14 | N-Acetyl-L-glutamate | M-H | Arginine biosynthesis |
| C01004 | 2 | 138.0550 | 81.8 | 0.0123 | 2.37 | N-Methylnicotinate | M + H | Nicotinate and nicotinamide metabolism |
| C00153 | 3 | 123.0553 | 58.7 | 0.0210 | −2.42 | Nicotinamide | M + H | Nicotinate and nicotinamide metabolism |
| C02862 | 2 | 232.1541 | 77.5 | 0.0178 | −1.78 | O-Butanoylcarnitine | M + H | |
| C03017 | 2 | 218.1386 | 82 | 0.0000 | −4.90 | O-Propionylcarnitine | M + H | |
| C00245 | 2 | 126.0220 | 78.9 | 0.0005 | −2.94 | Taurine | M + H | Neuroactive ligand-receptor interaction |

biosynthesis, and folate metabolism (Fig. 4). Although these groups include up- and down-regulated DEGs, members of carbon and fatty acid metabolism are primarily down-regulated; while N-glycan, glycosaminoglycan, and folate metabolisms are mainly upregulated. Furthermore, some enzymes related to sphingolipid and arachidonic acid metabolism are upregulated. The selected metabolites reflect these changes: there is a general downregulation of fatty acyls, glycerophospholipids and carboxylic acids, among other metabolites, and an upregulation of some metabolites such as leukotriene A4. A subset of representative correlated metabolites is presented in Fig. 5 (see full list of medium and high confidence annotated metabolites in Supplementary Table 2). Taking this broad view into account, it is worth noting that suggested alterations in the endoplasmic reticulum (ER) could underlie the observed metabolic changes. The ER is the main cellular compartment involved in protein trafficking and folding, among other functions. Failure in the adaptive capacity of the ER results in the activation of stress responses (Unfolded Protein Response) that in different contexts can result in the activation of proinflammatory pathways, metabolic alterations and increased proliferation [44–47]. Cancer cells illustrate many of these changes, for example, through the action of the transcription factor c-Myc, which interestingly appears to be upregulated in Tg.Old astrocytes based on transcriptomics data. ER stress-related alterations are also critical in chronic metabolic diseases such as obesity and type 2 diabetes, making them an interesting therapeutic target [48–50].

### 3.3. *Key metabolite alterations involved in astrocyte energetics and signaling*

The results presented indicate perturbations in essential centers of brain homeostasis, including energy metabolism, redox metabolism,

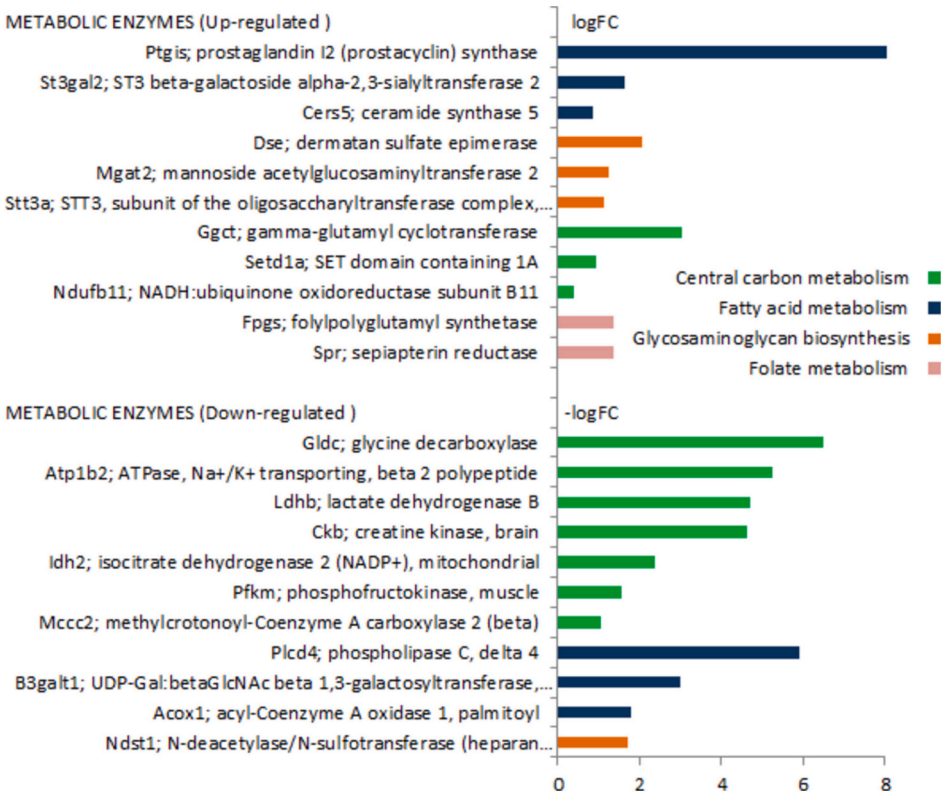


**Fig. 4.** Selected enzymes based on xMWAS association analysis between transcriptome and metabolome. Enzymes colored in blue are associated with the metabolism of fatty acids and related compounds (sphingolipids, glycosphingolipids, arachidonic acid); green: central carbon metabolism (oxidative phosphorylation, amino acid metabolism, etc.); orange: biosynthesis of N-glycans and glycosaminoglycans; violet: folate metabolism. For the sake of brevity, only a few representative members are shown. (For interpretation of the references to colour in this figure legend, the reader is referred to the web version of this article.)

signaling and inflammatory processes. In Fig. 5 we present some representative and confidently annotated metabolites that illustrate these changes. In this section we discuss the role and possible impact of these changes on homeostasis and the disease process. In particular, the change in the amino acid glutamate is probably one of the most relevant for astrocyte function [51,52] and this particular alteration was verified using a targeted approach (Fig. 6). Glutamate participates in a series of functions in the central nervous system, as an energy metabolite and neurotransmitter. Glutamate released by neurons is absorbed by astrocytes, where the enzyme glutamine synthetase converts it into glutamine and the latter returns to the neurons. In contrast, glutamine can be converted to glutamate by glutaminase (Gls). Consistent with the increased abundance of glutamate in neurotoxic astrocytes, this enzyme appears to be upregulated based on RNA-seq data [18]. Some of the accumulated glutamate may also undergo oxidative degradation. Glutamate imbalance is associated with neurotoxicity as it promotes oxidative stress and inflammation through different mechanisms such as direct interaction with the receptor and promotion of arachidonic acid metabolism or glutathione deprivation [53]. This phenomenon has been observed in various neurodegenerative diseases, including AD and amyotrophic lateral sclerosis (ALS) [54,55]. In this sense, the inhibition of glutaminase by compounds such as bis-2-(5-phenylacetamido-1,2,4-thiadiazol-2-yl)ethyl sulfide (BPTES) is an interesting therapeutic avenue. In addition to increased glutamate levels, altered levels of serine and tryptophan, among other metabolites, have been associated with inflammation and oxidative stress in the nervous system, a feature that could arise from increased amino acid catabolism [56–61].

In addition to the glutamate detected in the metabolomic study, we also specifically evaluated gamma aminobutyric acid (GABA), another important energy metabolite and neurotransmitter cycled between astrocytes and neurons, which has a higher abundance in neurotoxic astrocytes. Aberrant GABA production by monoamine oxidase-B (MAO-B) has been observed in reactive astrocytes and may be associated with memory impairment in murine models of AD [62,63]. Multiple MAO-B inhibitors have been proposed for the treatment of AD [64] supported by the fact that perturbations in this enzyme have been linked to AD and Parkinson's pathology [65,66]. In our previous study, we observed a notable increase in the level of MAO-B protein in 3xTg-AD neurotoxic astrocytes, although not statistically significant [14]. It has been hypothesized that increased GABA content in astrocytes could emerge in the early stages of AD as a coping mechanism to reduce plaque-mediated neuronal hyperactivity, so further research is needed to clarify its therapeutic potential [67,68].

Other high confidence annotations indicate a net decrease in the TCA intermediates, lactate and malate (pyruvate can be observed, but with a low confidence score) and possibly an increase in the pentose phosphate pathway metabolite, phosphoribosylpyrophosphate (PPP) (see Supplementary Material). PPP produces nicotinamide adenine dinucleotide phosphate, a cofactor necessary for restoration of reduced glutathione [69], cell growth and proliferation [70,71]. It can play a key role in regulating vascular function by altering the function of ion channels, promoting cell proliferation, improving cholesterol and fatty acid synthesis, modulating immune system function, and increasing oxidation [72]. In neurons it may have a protective function through its effect on oxidative stress [69,73].

Previous transcriptomic data suggested a shift from glycolysis to PPP (downregulation of Pfkp, Pfkp and Pfkfb3), along with a compensatory adjustment in the citric acid cycle toward anabolism (upregulation of Ldha and downregulation of Ldhb), glutaminolysis (positive regulation of Glul/GS) and alterations in the respiratory chain [18]. Of note, similar alterations can be observed in other cell types, particularly malignant cells [74–76]. A reduction in lactate is then unexpected, as suggested by the metabolomics results. However, these represent steady-state levels of metabolic intermediates and do not directly report associated fluxes,

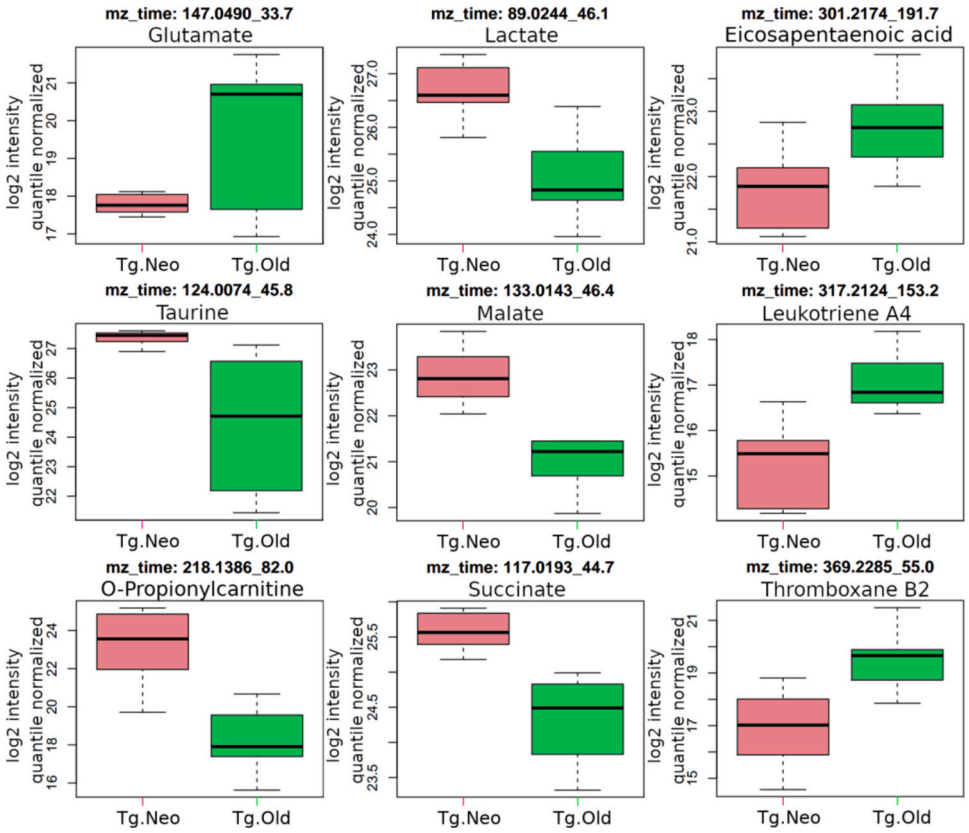


**Fig. 5.** Boxplot of selected metabolites from high-resolution metabolomics. The metabolites presented are a subset of metabolites correlated with the astrocytic transcriptomic profile based on xMWAS association analysis and with previously validated annotations and/or medium-high confidence annotations from xMSAnnotator. See the full list in Supplementary Table 2.

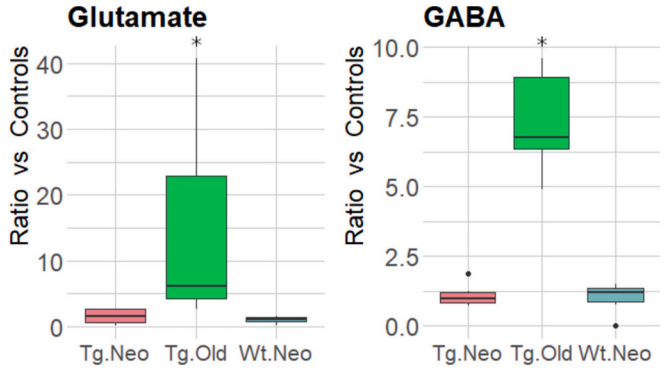


**Fig. 6.** Validated amino acid perturbations in astrocyte cell extracts (targeted analysis by HRMS). Pairwise comparisons using the Wilcoxon exact rank sum test, with Benjamini-Hochberg *p*-value adjustment procedure. *Adjusted *p*-value <0.05 for the comparison of Tg.Old versus Tg.Neo and Tg.Old versus Wt.Neo.

so their interpretation should be considered with caution. Although both results suggest a relative increase in PPP with respect to the glycolytic arm, the net balance between glycolysis and oxidative phosphorylation is more ambiguous. There is evidence of a decrease in some subunits of the respiratory chain complexes and a probable increase in the formation of supercomplexes that could have opposite effects [18]. These conflicts should be further evaluated through functional studies.

Our results also support a decrease in the protective metabolites carnitine and taurine against oxidative stress. Carnitine is an amino acid that transfers long-chain fatty acids to the mitochondrial matrix for β-oxidation, producing acetyl-CoA that then enters the TCA cycle. It helps reduce oxidative stress by preventing the accumulation of toxic long-chain acyl-CoA metabolites [77]. Decreases in carnitines and genes related to fatty acid metabolism have been associated with aging in human, mouse, and other animal models [77–80]. Population studies have linked carnitine depletion to an increased risk of memory impairment and Alzheimer's disease [81,82]. In this sense, supplementation with carnitines could have beneficial effects on senescence [83]. Taurine has been associated with a number of functions including energy metabolism, ER stress, neuromodulation and calcium homeostasis for which therapeutic potential has been proposed [84].

Another important alteration arising from our current results is in the metabolism of arachidonic acid (AA), which involves prostaglandins and other mediators of inflammatory responses (Table 1, Fig. 4). Annotated metabolites include eicosapentaenoic acid, leukotriene A4, and thromboxane B2, among others (Fig. 5, Supplementary Table 1). Neuroinflammation can have both positive and negative effects, and possible neuroprotective effects of certain AA metabolites through activation of the PPARgamma cascade have been described [85–87]. On the other hand, alterations in this cascade have been observed in AD and detrimental effects of the associated metabolites have been described in mouse models of the disease [88,89]. In addition to the detected metabolites, transcriptomics results indicate a perturbation of the enzymes Ptgis and Ptgs2 (Cox-2), among others, supporting an increase in the production of some of these mediators [18]. These were found among many altered mediators such as leucine-6 (Il-6), interleukin-33 (Il-33), C—C motif chemokine ligand 2 (Ccl2), and stromal cell-derived factor 1 (Cxcl12), among others, illustrating a complex proinflammatory profile with both beneficial, dual, or harmful effects on the nervous system [18].

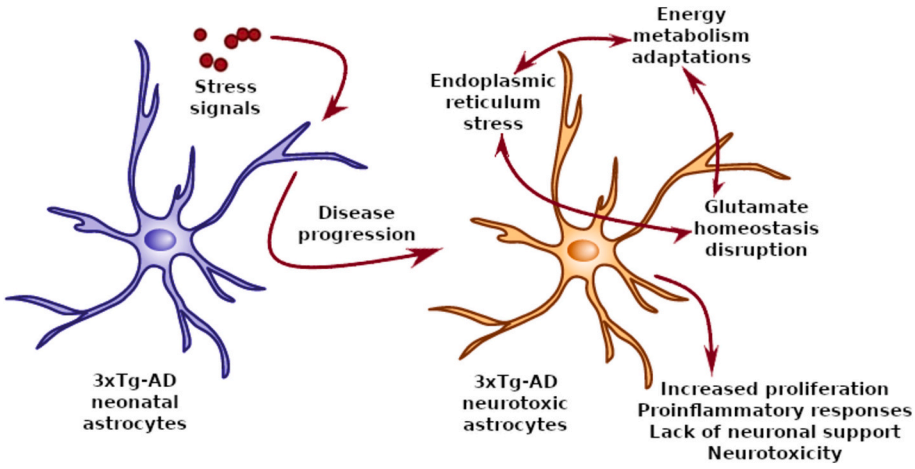


**Fig. 7.** Hypothetical mechanism underlying the phenotype of 3xTg-AD neurotoxic astrocytes.

## 4. Conclusions

To our knowledge, this is the first study to evaluate metabolic changes in astrocytes isolated from the 3xTg-AD mouse model. Our findings suggest important alterations in key energy and signaling centers of the brain, such as glutamate intermediates, GABA and TCA. These findings reinforce the concept that neurotoxic astrocytes could have compromised neuronal support capacity and/or directly have a deleterious effect through aberrant release of neurotransmitters. Furthermore, we observed an increase in proinflammatory mediators related to arachidonic acid metabolism. In a broader sense, our findings suggest that the previous alterations occur as part of a stress response triggered in the endoplasmic reticulum (Fig. 7). This response may not necessarily be harmful in its early stages, but constitutes a survival or damage control mechanism of astrocytes, since many of the annotated metabolites may have dual functions in the brain. Further investigations should be performed to confirm the existence of the suggested alterations, as well as the detection of additional alterations in vivo and their role in disease progression. Above all, our findings reinforce the value of astrocytes as a therapeutic target for neurodegenerative diseases.

## Funding

This work was supported by Agencia Nacional de Investigación e Innovación (ANII, Uruguay) through doctoral and mobility fellowships granted to Diego Carvalho [grant numbers POS_NAC_2017_1_140673, MOV_CA_2018_1_149736], by Comisión Académica de Posgrado (CAP) and by the Programa de Desarrollo de las Ciencias Básicas (PEDECIBA). Diego Carvalho, F. Arredondo, R. Dapueto, E. Savio and J.A. Abin Carriquiry are members of the National Research System (Sistema Nacional de Investigación, SNI, Uruguay). This work was supported by National Institute on Aging, R21 AG080247 granted to Dean Jones and Young-Mi Go, and National Institute of Neurological Disorders and Stroke RF1 NS130713 granted to Dean Jones.

## Ethical approval

All experimental procedures were approved by the Institutional Animal Ethics Committee (CEUA-CUDIM) as established by the National Committee of Animal Experimentation (CNEA), Montevideo, Uruguay.

## CRediT authorship contribution statement

**Diego Carvalho:** Writing – review & editing, Writing – original draft, Methodology, Investigation, Funding acquisition, Formal analysis, Data curation, Conceptualization. **Pablo Diaz-Amarilla:** Methodology, Investigation, Conceptualization. **Mathew R. Smith:** Writing – review & editing, Supervision, Methodology, Formal analysis. **María Daniela Santi:** Writing – review & editing, Investigation. **Marcela Martinez-Busi:** Investigation, Formal analysis. **Young-Mi Go:** Supervision, Methodology, Formal analysis. **Dean P. Jones:** Supervision, Methodology, Formal analysis. **Pablo Duarte:** Resources. **Eduardo Savio:** Supervision, Resources, Funding acquisition. **Juan A. Abin-Carriquiry:** Writing – review & editing, Supervision, Methodology, Funding acquisition, Formal analysis, Conceptualization. **Florencia Arredondo:** Writing – review & editing, Supervision, Methodology, Investigation, Funding acquisition, Formal analysis, Conceptualization.

## Declaration of competing interest

The authors declare that they have no known competing financial interests or personal relationships that could have appeared to influence the work reported in this article.

## Acknowledgments

We would like to thank all the team of CUDIM SPF centralized animal facility for their fundamental work in animal care and assistance lead by Dr. Fabiana Isaurralde and formerly Dr. Silvia Hernandez. This work is supported by Metabolomics Workbench/National Metabolomics Data Repository (NMDR) (grant# U2C-DK119886), Common Fund Data Ecosystem (CFDE) (grant# 3OT2OD030544) and Metabolomics Consortium Coordinating Center (M3C) (grant# 1U2C-DK119889).

## Appendix A. Supplementary data

Supplementary data to this article can be found online at https://doi.org/10.1016/j.jprot.2024.105336.

## Data availability

The data access path is provided in the text of our manuscript.

## References

[1] K. Blennow, M.J. de Leon, H. Zetterberg, H.W. Querfurth, F.M. LaFerla, Alzheimer's disease, Lancet 368 (2006) 387–403, https://doi.org/10.1016/S0140-6736(06)69113-7.
[2] C. Reitz, R. Mayeux, Alzheimer disease: epidemiology, diagnostic criteria, risk factors and biomarkers, Biochem. Pharmacol. 88 (2014) 640–651, https://doi.org/10.1016/j.bcp.2013.12.024.
[3] D.J. Selkoe, J. Hardy, The amyloid hypothesis of Alzheimer's disease at 25 years, EMBO Mol. Med. 8 (2016) 595–608, https://doi.org/10.15252/emmm.201606210.

[4] M.T. Heneka, M.J. Carson, J. El Khoury, G.E. Landreth, F. Brosseron, D.L. Feinstein, A.H. Jacobs, T. Wyss-Coray, J. Vitorica, R.M. Ransohoff, K. Herrup, S.A. Frautschy, B. Finsen, G.C. Brown, A. Verkhratsky, K. Yamanaka, J. Koistinaho, E. Latz, A. Halle, G.C. Petzold, T. Town, D. Morgan, M.L. Shinohara, V.H. Perry, C. Holmes, N.G. Bazan, D.J. Brooks, S. Hunot, B. Joseph, N. Deigendesch, O. Garaschuk, E. Boddeke, C.A. Dinarello, J.C. Breitner, G.M. Cole, D.T. Golenbock, M. P. Kummer, Neuroinflammation in Alzheimer's disease, Lancet Neurol. 14 (2015) 388, https://doi.org/10.1016/S1474-4422(15)70016-5.
[5] B.V. Zlokovic, Neurovascular mechanisms of Alzheimer's neurodegeneration, Trends Neurosci. 28 (2005) 202–208, https://doi.org/10.1016/J.TINS.2005.02.001.
[6] E. Trushina, T. Dutta, X.T. Persson, M.M. Mielke, R.C. Petersen, Identification of altered metabolic pathways in plasma and CSF in mild cognitive impairment and Alzheimer's disease using, Metabolomics 8 (2013), https://doi.org/10.1371/journal.pone.0063644.
[7] M.V. Sofroniew, H.V. Vinters, Astrocytes: biology and pathology, Acta Neuropathol. 119 (2010) 7–35, https://doi.org/10.1007/S00401-009-0619-8/FIGURES/9.
[8] M.V. Sofroniew, Astrocyte reactivity: subtypes, states, and functions in CNS innate immunity, Trends Immunol. 41 (2020) 758–770, https://doi.org/10.1016/J.IT.2020.07.004.
[9] P. Díaz-Amarilla, S. Olivera-Bravo, E. Trias, A. Cragnolini, L. Martínez-Palma, P. Cassina, J. Beckman, L. Barbeito, Phenotypically aberrant astrocytes that promote motoneuron damage in a model of inherited amyotrophic lateral sclerosis, Proc. Natl. Acad. Sci. USA 108 (2011) 18126–18131, https://doi.org/10.1073/pnas.1110689108.
[10] S.A. Liddelow, B.A. Barres, Reactive astrocytes: production, function, and therapeutic potential, Immunity 46 (2017) 957–967, https://doi.org/10.1016/j.immuni.2017.06.006.
[11] R. Siracusa, R. Fusco, S. Cuzzocrea, Astrocytes: role and functions in brain pathologies, Front. Pharmacol. 0 (2019) 1114, https://doi.org/10.3389/FPHAR.2019.01114.
[12] M. van Gijsel-Bonnello, K. Baranger, P. Benech, S. Rivera, M. Khrestchatisky, M. de Reggi, B. Gharib, Metabolic changes and inflammation in cultured astrocytes from the 5xFAD mouse model of Alzheimer's disease: alleviation by pantethine, PLoS One 12 (2017) e0175369, https://doi.org/10.1371/journal.pone.0175369.
[13] R. Medeiros, F.M. LaFerla, Astrocytes: conductors of the Alzheimer disease neuroinflammatory symphony, Exp. Neurol. 239 (2013) 133–138, https://doi.org/10.1016/j.expneurol.2012.10.007.
[14] P. Diaz-Amarilla, F. Arredondo, R. Dapueto, V. Boix, D. Carvalho, M.D. Santi, E. Vasilskis, R. Mesquita-Ribeiro, F. Dajas-Bailador, J.A. Abin-Carriquiry, H. Engler, E. Savio, Isolation and characterization of neurotoxic astrocytes derived from old triple transgenic Alzheimer's disease mice, Neurochem. Int. 159 (2022), https://doi.org/10.1016/j.neuint.2022.105403.
[15] S. Li, A. Todor, R. Luo, Blood transcriptomics and metabolomics for personalized medicine, Comput. Struct, Biotechnol. J. 14 (2016) 1–7, https://doi.org/10.1016/J.CSBJ.2015.10.005.
[16] K. Man, V.I. Kutyavin, A. Chawla, Tissue Immunometabolism: development, physiology, and pathobiology, Cell Metab. 25 (2017) 11–26, https://doi.org/10.1016/J.CMET.2016.08.016.
[17] A.S. Husted, M. Trauelsen, O. Rudenko, S.A. Hjorth, T.W. Schwartz, GPCR-mediated signaling of metabolites, Cell Metab. 25 (2017) 777–796, https://doi.org/10.1016/J.CMET.2017.03.008.
[18] D. Carvalho, P. Diaz-Amarilla, R. Dapueto, M.D. Santi, P. Duarte, E. Savio, H. Engler, J.A. Abin-Carriquiry, F. Arredondo, Transcriptomic analyses of neurotoxic astrocytes derived from adult triple transgenic Alzheimer's disease mice, J. Mol. Neurosci. 2023 (2023) 1–29, https://doi.org/10.1007/S12031-023-02105-2.
[19] S. Oddo, A. Caccamo, J.D. Shepherd, M.P. Murphy, T.E. Golde, R. Kayed, R. Metherate, M.P. Mattson, Y. Akbari, F.M. LaFerla, Triple-transgenic model of Alzheimer's disease with plaques and tangles: intracellular Abeta and synaptic dysfunction, Neuron 39 (2003) 409–421, https://doi.org/10.1016/S0896-6273(03)00434-3.
[20] J.C. Carroll, E.R. Rosario, S. Kreimer, A. Villamagna, E. Gentzschein, F.Z. Stanczyk, C.J. Pike, Sex differences in β-amyloid accumulation in 3xTg-AD mice: role of neonatal sex steroid hormone exposure, Brain Res. 1366 (2010) 233–245, https://doi.org/10.1016/J.BRAINRES.2010.10.009.
[21] L.K. Clinton, L.M. Billings, K.N. Green, A. Caccamo, J. Ngo, S. Oddo, J.L. McGaugh, F.M. LaFerla, Age-dependent sexual dimorphism in cognition and stress response in the 3xTg-AD mice, Neurobiol. Dis. 28 (2007) 76–82, https://doi.org/10.1016/J.NBD.2007.06.013.
[22] P. Cassina, H. Peluffo, M. Pehar, L. Martinez-Palma, A. Ressia, J.S. Beckman, A. G. Estévez, L. Barbeito, Peroxynitrite triggers a phenotypic transformation in spinal cord astrocytes that induces motor neuron apoptosis, J. Neurosci. Res. 67 (2002) 21–29, https://doi.org/10.1002/jnr.10107.
[23] Y.M. Go, C.W. Kim, D.I. Walker, D.W. Kang, S. Kumar, M. Orr, K. Uppal, A. A. Quyyumi, H. Jo, D.P. Jones, Disturbed flow induces systemic changes in metabolites in mouse plasma: a metabolomics study using apoe−/− mice with partial carotid ligation, Am. J. Phys. Regul. Integr. Comp. Phys. 308 (2015) R62–R72, https://doi.org/10.1152/ajpregu.00278.2014.
[24] S.C. Sapcariu, T. Kanashova, D. Weindl, J. Ghelfi, G. Dittmar, K. Hiller, Simultaneous extraction of proteins and metabolites from cells in culture, MethodsX 1 (2014) 74–80, https://doi.org/10.1016/j.mex.2014.07.002.
[25] K.H. Liu, M. Nellis, K. Uppal, C. Ma, V.L. Tran, Y. Liang, D.I. Walker, D.P. Jones, Reference standardization for quantification and harmonization of large-scale metabolomics, Anal. Chem. 92 (2020) 8836–8844, https://doi.org/10.1021/acs.analchem.0c00338.
[26] Q.A. Soltow, F.H. Strobel, K.G. Mansfield, L. Wachtman, Y. Park, D.P. Jones, High-performance metabolic profiling with dual chromatography-Fourier-transform mass spectrometry (DC-FTMS) for study of the exposome, Metabolomics 9 (2013) 132–143, https://doi.org/10.1007/s11306-011-0332-1.
[27] J.K. Frediani, D.P. Jones, N. Tukvadze, K. Uppal, E. Sanikidze, M. Kipiani, V. T. Tran, G. Hebbar, D.I. Walker, R.R. Kempker, S.S. Kurani, R.A. Colas, J. Dalli, V. Tangpricha, C.N. Serhan, H.M. Blumberg, T.R. Ziegler, Plasma metabolomics in human pulmonary tuberculosis disease: a pilot study, PLoS One 9 (2014), https://doi.org/10.1371/journal.pone.0108854.
[28] K.H. Liu, D.I. Walker, K. Uppal, V.L. Tran, P. Rohrbeck, T.M. Mallon, D.P. Jones, High-resolution metabolomics assessment of military personnel evaluating analytical strategies for chemical detection, J. Occup. Environ. Med. 58 (2016) S53–S61, https://doi.org/10.1097/JOM.0000000000000773.
[29] M. Sud, E. Fahy, D. Cotter, K. Azam, I. Vadivelu, C. Burant, A. Edison, O. Fiehn, R. Higashi, K.S. Nair, S. Sumner, S. Subramaniam, Metabolomics workbench: An international repository for metabolomics data and metadata, metabolite standards, protocols, tutorials and training, and analysis tools, Nucleic Acids Res. 44 (2016) D463–D470, https://doi.org/10.1093/nar/gkv1042.
[30] T. Yu, Y. Park, J.M. Johnson, D.P. Jones, apLCMS-adaptive processing of high-resolution LC/MS data, Bioinformatics 25 (2009) 1930–1936, https://doi.org/10.1093/bioinformatics/btp291.
[31] K. Uppal, Q.A. Soltow, F.H. Strobel, W.S. Pittard, K.M. Gernert, T. Yu, D.P. Jones, XMSanalyzer: automated pipeline for improved feature detection and downstream analysis of large-scale, non-targeted metabolomics data, BMC Bioinformatics. 14 (2013) 1–12, https://doi.org/10.1186/1471-2105-14-15.
[32] S.M. Kohl, M.S. Klein, J. Hochrein, P.J. Oefner, R. Spang, W. Gronwald, State-of-the art data normalization methods improve NMR-based metabolomic analysis, Metabolomics 8 (2012) 146–160, https://doi.org/10.1007/s11306-011-0350-z.
[33] M.E. Ritchie, B. Phipson, D. Wu, Y. Hu, C.W. Law, W. Shi, G.K. Smyth, Limma powers differential expression analyses for RNA-sequencing and microarray studies, Nucleic Acids Res. 43 (2015) e47, https://doi.org/10.1093/nar/gkv007.
[34] Y. Hochberg, Y. Benjamini, More powerful procedures for multiple significance testing, Stat. Med. 9 (1990) 811–818, https://doi.org/10.1002/sim.4780090710.
[35] M. Kanehisa, M. Furumichi, Y. Sato, M. Ishiguro-Watanabe, M. Tanabe, KEGG: integrating viruses and cellular organisms, Nucleic Acids Res. 49 (2021) D545–D551, https://doi.org/10.1093/NAR/GKAA970.
[36] D.S. Wishart, T. Jewison, A.C. Guo, M. Wilson, C. Knox, Y. Liu, Y. Djoumbou, R. Mandal, F. Aziat, E. Dong, S. Bouatra, I. Sinelnikov, D. Arndt, J. Xia, P. Liu, F. Yallou, T. Bjorndahl, R. Perez-Pineiro, R. Eisner, F. Allen, V. Neveu, R. Greiner, A. Scalbert, HMDB 3.0-the human metabolome database in 2013, Nucleic Acids Res. 41 (2013), https://doi.org/10.1093/nar/gks1065.
[37] K. Uppal, D.I. Walker, D.P. Jones, xMSannotator: An R package for network-based annotation of high-resolution metabolomics data, Anal. Chem. 89 (2017) 1063–1067, https://doi.org/10.1021/acs.analchem.6b01214.
[38] S. Li, Y. Park, S. Duraisingham, F.H. Strobel, N. Khan, Q.A. Soltow, D.P. Jones, B. Pulendran, Predicting network activity from high throughput metabolomics, PLoS Comput. Biol. 9 (2013) 1003123, https://doi.org/10.1371/journal.pcbi.1003123.
[39] K. Uppal, C. Ma, Y.M. Go, D.P. Jones, XMWAS: a data-driven integration and differential network analysis tool, Bioinformatics 34 (2018) 701–702, https://doi.org/10.1093/bioinformatics/btx656.
[40] H. Chun, S. Keleş, Sparse partial least squares regression for simultaneous dimension reduction and variable selection, J. R. Stat. Soc. Ser. B Stat Methodol. 72 (2010) 3–25, https://doi.org/10.1111/j.1467-9868.2009.00723.x.
[41] V.D. Blondel, J.L. Guillaume, R. Lambiotte, E. Lefebvre, Fast unfolding of communities in large networks, J. Stat. Mech. Theory Exp. 2008 (2008) P10008, https://doi.org/10.1088/1742-5468/2008/10/P10008.
[42] J. Lozano, S. Fernández-Ciganda, Á. González Revello, D. Hirigoyen, M. Martínez, C. Scorza, P. Zunino, Probiotic potential of GABA-producing lactobacilli isolated from Uruguayan artisanal cheese starter cultures, J. Appl. Microbiol. 133 (2022), https://doi.org/10.1111/jam.15664.
[43] Z. Pang, J. Chong, G. Zhou, D.A. de Lima Morais, L. Chang, M. Barrette, C. Gauthier, P.-É. Jacques, S. Li, J. Xia, MetaboAnalyst 5.0: narrowing the gap between raw spectra and functional insights, Nucleic Acids Res. (2021), https://doi.org/10.1093/nar/gkab382.
[44] N.T. Sprenkle, S.G. Sims, C.L. Sánchez, G.P. Meares, Endoplasmic reticulum stress and inflammation in the central nervous system, Mol. Neurodegener. 121 (12) (2017) 1–18, https://doi.org/10.1186/S13024-017-0183-Y.
[45] D.M. Miller, S.D. Thomas, A. Islam, D. Muench, K. Sedoris, C-Myc and Cancer metabolism, Clin. Cancer Res. 18 (2012) 5546–5553, https://doi.org/10.1158/1078-0432.CCR-12-0977.
[46] X. Sheng, H.Z. Nenseth, S. Qu, O.F. Kuzu, T. Frahnow, L. Simon, S. Greene, Q. Zeng, L. Fazli, P.S. Rennie, I.G. Mills, H. Danielsen, F. Theis, J.B. Patterson, Y. Jin, F. Saatcioglu, IRE1α-XBP1s pathway promotes prostate cancer by activating c-MYC signaling, Nat. Commun. 101 (10) (2019) 1–12, https://doi.org/10.1038/s41467-018-08152-3.
[47] T. Zhang, N. Li, C. Sun, Y. Jin, X. Sheng, MYC and the unfolded protein response in cancer: synthetic lethal partners in crime? EMBO Mol. Med. 12 (2020) https://doi.org/10.15252/EMMM.201911845.
[48] G.S. Hotamisligil, Endoplasmic reticulum stress and the inflammatory basis of metabolic disease, Cell 140 (2010) 900–917, https://doi.org/10.1016/J.CELL.2010.02.034.

[49] R.K. Yadav, S.-W. Chae, H.-R. Kim, H.J. Chae, H.J. Chae, H.J. Chae, Endoplasmic reticulum stress and Cancer, J. Cancer Prev. 19 (2014) 75–88, https://doi.org/10.15430/JCP.2014.19.2.75.
[50] C.A. Martin-Jiménez, Á. García-Vega, R. Cabezas, G. Aliev, V. Echeverria, J. González, G.E. Barreto, Astrocytes and endoplasmic reticulum stress: a bridge between obesity and neurodegenerative diseases, Prog. Neurobiol. 158 (2017) 45–68, https://doi.org/10.1016/J.PNEUROBIO.2017.08.001.
[51] P.J. Magistretti, Neuron-glia metabolic coupling and plasticity, J. Exp. Biol. 209 (2006) 2304–2311, https://doi.org/10.1242/jeb.02208.
[52] L. Hertz, D.L. Rothman, Glutamine-glutamate cycle flux is similar in cultured astrocytes and brain and both glutamate production and oxidation are mainly catalyzed by aspartate aminotransferase, Biology (Basel). 6 (2017), https://doi.org/10.3390/biology6010017.
[53] F. Herrera, R.M. Sainz, J.C. Mayo, V. Martín, I. Antolín, C. Rodriguez, Glutamate induces oxidative stress not mediated by glutamate receptors or cystine transporters: protective effect of melatonin and other antioxidants, J. Pineal Res. 31 (2001) 356–362, https://doi.org/10.1034/J.1600-079X.2001.310411.X.
[54] D. Schubert, D. Piasecki, Oxidative glutamate toxicity can be a component of the excitotoxicity Cascade, J. Neurosci. 21 (2001) 7455–7462, https://doi.org/10.1523/JNEUROSCI.21-19-07455.2001.
[55] C.E. Shaw, A. Al-Chalabi, N. Leigh, Progress in the pathogenesis of amyotrophic lateral sclerosis, Curr. Neurol. Neurosci. Reports 11 (1) (2001) 69–76, https://doi.org/10.1007/S11910-001-0078-7.
[56] K.Y. Kim, S.K. Hwang, S.Y. Park, M.J. Kim, D.Y. Jun, Y.H. Kim, L-serine protects mouse hippocampal neuronal HT22 cells against oxidative stress-mediated mitochondrial damage and apoptotic cell death, Free Radic. Biol. Med. 141 (2019) 447–460, https://doi.org/10.1016/J.FREERADBIOMED.2019.07.018.
[57] M. Hajsl, A. Hlavackova, K. Broulikova, M. Sramek, M. Maly, J.E. Dyr, J. Suttnar, Tryptophan Metabolism, Inflammation, and Oxidative Stress in Patients with Neurovascular Disease, Metab 10 (2020) 208, https://doi.org/10.3390/METABO10050208.
[58] I. Davis, A. Liu, What is the tryptophan kynurenine pathway and why is it important to neurotherapeutics? Doi:10.1586/14737175.2015.1049999. 15 (2015) 719–721, https://doi.org/10.1586/14737175.2015.1049999.
[59] J.W.D. Griffin, P.C. Bradshaw, Amino acid catabolism in Alzheimer's disease brain: friend or foe? Oxidative Med. Cell. Longev. 2017 (2017) 5472792, https://doi.org/10.1155/2017/5472792.
[60] H.S. Waagepetersen, U. Sonnewald, A. Schousboe, Energy and amino acid neurotransmitter metabolism in astrocytes, Astrocytes (Patho)physiology Nerv. Syst 9780387794921 (2009) 177–200, https://doi.org/10.1007/978-0-387-79492-1_7.
[61] T.W. Tefera, K. Borges, Neuronal glucose metabolism is impaired while astrocytic TCA cycling is unaffected at symptomatic stages in the hSOD1G93A mouse model of amyotrophic lateral sclerosis, Doi:10.1177/0271678X18764775 39 (2018) 1710–1724, https://doi.org/10.1177/0271678X18764775.
[62] H. Chun, H. An, J. Lim, J. Woo, J. Lee, H. Ryu, C.J. Lee, C. H, A. H, L.L. J, W. J, L.L. J, R. H, L. CJ, H. Chun, H. An, J. Lim, J. Woo, J. Lee, H. Ryu, C.J. Lee, C. H, A. H, L. L. J, W. J, L.L. J, R. H, L. CJ, Astrocytic proBDNF and tonic GABA distinguish active versus reactive astrocytes in Hippocampus, Exp. Neurobiol. 27 (2018) 155, https://doi.org/10.5607/EN.2018.27.3.155.
[63] S. Jo, O. Yarishkin, Y.J. Hwang, Y.E. Chun, M. Park, D.H. Woo, J.Y. Bae, T. Kim, J. Lee, H. Chun, H.J. Park, D.Y. Lee, J. Hong, H.Y. Kim, S.-J.J. Oh, S.J. Park, H. Lee, B.-E.E. Yoon, Y. Kim, Y. Jeong, I. Shim, Y.C. Bae, J. Cho, N.W. Kowall, H. Ryu, E. Hwang, D. Kim, C.J. Lee, GABA from reactive astrocytes impairs memory in mouse models of Alzheimer's disease, Nat. Med. 208 (20) (2014) 886–896, https://doi.org/10.1038/nm.3639.
[64] T. Behl, D. Kaur, A. Sehgal, S. Singh, N. Sharma, G. Zengin, F.L. Andronie-Cioara, M.M. Toma, S. Bungau, A.G. Bumbu, Role of Monoamine Oxidase Activity in Alzheimer's Disease: An Insight into the Therapeutic Potential of Inhibitors, Mol 26 (2021) 3724, https://doi.org/10.3390/MOLECULES26123724.
[65] B. Gulyás, E. Pavlova, P. Kása, K. Gulya, L. Bakota, S. Várszegi, É. Keller, M. C. Horváth, S. Nag, I. Hermecz, K. Magyar, C. Halldin, Activated MAO-B in the brain of Alzheimer patients, demonstrated by [11C]-l-deprenyl using whole hemisphere autoradiography, Neurochem. Int. 58 (2011) 60–68, https://doi.org/10.1016/J.NEUINT.2010.10.013.
[66] H. An, J.Y. Heo, C.J.L, M.-H. Nam, The pathological role of astrocytic MAOB in parkinsonism revealed by genetic ablation and over-expression of MAOB, Exp. Neurobiol. 30 (2021) 113–119, https://doi.org/10.5607/EN21007.
[67] B.T. Assefa, A.K. Gebre, B.M. Altaye, Reactive astrocytes as drug target in Alzheimer's disease, Biomed. Res. Int. 2018 (2018), https://doi.org/10.1155/2018/4160247.
[68] C. Acioglu, L. Li, S. Elkabes, Contribution of astrocytes to neuropathology of neurodegenerative diseases, Brain Res. 1758 (2021) 147291, https://doi.org/10.1016/J.BRAINRES.2021.147291.
[69] J.P. Bolaños, A. Almeida, The pentose-phosphate pathway in neuronal survival against nitrosative stress, IUBMB Life 62 (2010) 14–18, https://doi.org/10.1002/IUB.280.
[70] E.S. Cho, Y.H. Cha, H.S. Kim, N.H. Kim, J.I. Yook, The pentose phosphate pathway as a potential target for cancer therapy, Biomol. Ther. 26 (2018) 29–38, https://doi.org/10.4062/biomolther.2017.179.
[71] L. Hertz, L. Peng, G.A. Dienel, Energy metabolism in astrocytes: high rate of oxidative metabolism and spatiotemporal dependence on glycolysis/glycogenolysis, J. Cereb. Blood Flow Metab. 27 (2007) 219–249, https://doi.org/10.1038/sj.jcbfm.9600343.
[72] S.A. Gupte, Targeting the pentose phosphate pathway in syndrome X-related cardiovascular complications, Drug Dev. Res. 71 (2010) 161–167, https://doi.org/10.1002/DDR.20359.
[73] B.N. Manolescu, M. Berteanu, E. Oprea, N. Chiriac, L. Dumitru, S. Vlădoiu, O. Popa, O. Ianăş, Dynamic of oxidative and nitrosative stress markers during the convalescent period of stroke patients undergoing rehabilitation, Doi:10.1258/Acb.2011.010243 48 (2011) 338–343, https://doi.org/10.1258/ACB.2011.010243.
[74] C.J. Valvona, H.L. Fillmore, P.B. Nunn, G.J. Pilkington, The regulation and function of lactate dehydrogenase a: therapeutic potential in brain tumor, Brain Pathol. 26 (2016) 3–17, https://doi.org/10.1111/BPA.12299.
[75] Z.H. Wang, W.B. Peng, P. Zhang, X.P. Yang, Q. Zhou, Lactate in the tumour microenvironment: from immune modulation to therapy, EBioMedicine 73 (2021), https://doi.org/10.1016/J.EBIOM.2021.103627.
[76] Y. Chinchore, T. Begaj, D. Wu, E. Drokhlyansky, C.L. Cepko, Glycolytic reliance promotes anabolism in photoreceptors, Elife 6 (2017), https://doi.org/10.7554/ELIFE.25946.
[77] D. Derous, S.E. Mitchell, C.L. Green, Y. Wang, J.D.J. Han, L. Chen, D.E. L. Promislow, D. Lusseau, A. Douglas, J.R. Speakman, The effects of graded levels of calorie restriction: X. Transcriptomic Responses of Epididymal Adipose Tissue, Journals Gerontol. Ser. A. 73 (2018) 279–288, https://doi.org/10.1093/GERONA/GLX101.
[78] R.H. Houtkooper, C. Argmann, S.M. Houten, C. Cantó, E.H. Jeninga, P.A. Andreux, C. Thomas, R. Doenlen, K. Schoonjans, J. Auwerx, The metabolic footprint of aging in mice, Sci. Report. 2011 11. 1 1–11. doi:https://doi.org/10.1038/srep00134.
[79] J.M. Hoffman, Q.A. Soltow, S. Li, A. Sidik, D.P. Jones, D.E.L. Promislow, Effects of age, sex, and genotype on high-sensitivity metabolomic profiles in the fruit fly, Drosophila melanogaster, Aging Cell 13 (2014) 596–604, https://doi.org/10.1111/ACEL.12215.
[80] L.A. Gómez, S.H.D. Heath, T.M. Hagen, Acetyl-l-carnitine supplementation reverses the age-related decline in carnitine palmitoyltransferase 1 (CPT1) activity in interfibrillar mitochondria without changing the l-carnitine content in the rat heart, Mech. Ageing Dev. 133 (2012) 99–106, https://doi.org/10.1016/J.MAD.2012.01.007.
[81] I. Hajjar, Q. Cai, T. Yu, D.P. Jones, Untargeted Metabolomics Shows Alterations in Homocysteine, Lipids and Fatty Acids predicting Memory Decline in Healthy Middle-Aged Individuals, BioRxiv, 2020, https://doi.org/10.1101/2020.02.23.949537, 2020.02.23.949537.
[82] M. Lodeiro, C. Ibáñez, A. Cifuentes, C. Simó, Á. Cedazo-Mínguez, Decreased cerebrospinal fluid levels of L-carnitine in non-apolipoprotein E4 carriers at early stages of Alzheimer's disease, J. Alzheimers Dis. 41 (2014) 223–232, https://doi.org/10.3233/JAD-132063.
[83] R.C. Noland, T.R. Koves, S.E. Seiler, H. Lum, R.M. Lust, O. Ilkayeva, R.D. Stevens, F.G. Hegardt, D.M. Muoio, Carnitine insufficiency caused by aging and Overnutrition compromises mitochondrial performance and metabolic control *, J. Biol. Chem. 284 (2009) 22840–22852, https://doi.org/10.1074/JBC.M109.032888.
[84] S. Schaffer, H.W. Kim, Effects and mechanisms of taurine as a therapeutic agent, Biomol. Ther. (Seoul). 26 (2018) 225–241, https://doi.org/10.4062/BIOMOLTHER.2017.251.
[85] L. Sun, Y.-W. Xu, J. Han, H. Liang, N. Wang, Y. Cheng, S. L, X. YW, H. J, L. H, W. N, C. Y, 12/15-Lipoxygenase metabolites of arachidonic acid activate PPARγ: a possible neuroprotective effect in ischemic brain 56, 2015, pp. 502–514, https://doi.org/10.1194/JLR.M053058.
[86] Z.J. Wang, C.L. Liang, G.M. Li, C.Y. Yu, M. Yin, W. ZJ, L. CL, L. GM, Y. CY, Y. M, Neuroprotective effects of arachidonic acid against oxidative stress on rat hippocampal slices 163, 2006, pp. 207–217, https://doi.org/10.1016/J.CBI.2006.08.005.
[87] V. Sambra, F. Echeverria, A. Valenzuela, R. Chouinard-Watkins, R. Valenzuela, Docosahexaenoic and Arachidonic Acids as Neuroprotective Nutrients throughout the Life Cycle, Nutr 13 (2021) 986, https://doi.org/10.3390/NU13030986.
[88] Z. Amtul, M. Uhrig, L. Wang, R.F. Rozmahel, K. Beyreuther, Detrimental effects of arachidonic acid and its metabolites in cellular and mouse models of Alzheimer's disease: structural insight, Neurobiol. Aging 33 (831) (2012), https://doi.org/10.1016/J.NEUROBIOLAGING.2011.07.014 e21–831.e31.
[89] M.H. Thomas, J.L. Olivier, Arachidonic acid in Alzheimer's disease, J. Neurol. Neuromedicine. 1 (2016) 1–6. www.jneurology.com (accessed August 2, 2021).